Rheological properties of alumina powder mixtures investigated using shear tests

Guillaume Bernard-Granger, Martin Giraud, Elodie Pascal, Loïc Mailhan, Timo Larsson, Christophe Valot, Carine Ablitzer, Cendrine Gatumel, Henri Berthiaux

Rheological properties of alumina powder mixtures investigated using shear tests

Guillaume Bernard-Granger [a,*], Martin Giraud [a], Elodie Pascal [a], Loïc Mailhan [a], Timo Larsson [a], Christophe Valot [a], Carine Ablitzer [b], Cendrine Gatumel [c], Henri Berthiaux [c]

[a] CEA, Nuclear Energy Division, Research Department on Mining and Fuel Recycling Processes, 30207 Bagnols-sur-Cèze, France
[b] CEA, Nuclear Energy Division, Fuel Studies Department, 13115 Saint-Paul-lez-Durance, France
[c] Laboratoire RAPSODEE, UMR CNRS 5302, Ecole des Mines d'Albi-Carmaux, Campus Jarlard, 81013 Albi Cedex 09, France

A B S T R A C T

The flow properties of alumina powder mixtures have been investigated using shear tests on a powder rheometer. The evolution of the flow index, ff_c, as a function of the powder mixture composition show that all the points form a single curve whatever the pre-shear consolidation stress value adopted, the mixing conditions and the preconditioning of the powder bed (relative humidity) before the tests. It has been also shown that the flow properties of the mixtures are controlled by the competition between the inter-particle interaction forces (Van der Waals and capillary contributions) and gravity via the Bond number.

Keywords:
Powder mixtures
alumina
cohesion
flow index
Bond number

1. Introduction

A lot of industries are manufacturing final products using powders as the material source. For example, in the nuclear industry, the fuel pellets are shaped by automatic uniaxial pressing from a powder and sintered in a second step. In the pharmaceutical industry drug pills are shaped on rotary tablet presses from powdered formulations. In both cases, the powdered media must have optimal and robust flow properties to fill the molds with the adequate mass of matter to ensure a high throughput of manufactured green parts with the lowest amount as possible of detrimental defects (chips, cracks, end-capping effect, non-respect of dimensions and weight…). Such powdered media are stored in hoppers or containers before being transferred towards the pressing tools using, for example, worm driving, gravitational transfer, pneumatic transfer, conveyor belts or a combination of several of these possibilities. Behind that, the powdered media may be manufactured/conditioned using batch methods (ball milling, homogenization procedures in blenders for example) without any retention issue during the emptying operations. Then, most of the time such powdered media are put into motion, namely flowing, from a stationary consolidated state at some point of the manufacturing process.

To investigate the flow properties of a consolidated powder medium or bulk solid, shear-cell tests are used [1–4]. It enables the construction of a yield locus associated to a pre-shear point for a steady-state flow. The flow properties are then investigated by measuring two sets of data points [1,2]: a) a pre-shear point which corresponds to the pair of normal and shear stresses (σ_{SF}, τ_{SF}), represented by the red square on Fig. 1, leading to a steady-state flow under a pre-selected normal stress σ_{SF}, b) a collection of pairs (σ, τ) at incipient flow, represented by the dark squares on Fig. 1, measured on the same powdered sample repeatedly pre-consolidated under σ_{SF}. If the investigated material behaves as an ideal Coulomb one, the yield locus can be linearized as follows [5] (dark-dotted line on Fig. 1):

$$\tau = \mu\sigma + c \tag{1}$$

where τ and σ are respectively the shear and normal stresses at yield exerted on the medium investigated, μ is the static inter-particle friction coefficient and c is named cohesion. Cohesion may be seen as the powder bed shear resistance under a normal compressive stress set to zero. Regarding Relation (1), at the contact scale all the friction phenomena between particles are taken into account by the term $\mu\sigma$ and all the other interaction phenomena (electrostatic, capillary and Van der Waals forces) between particles beyond friction are encompassed in c. From the yield locus and the pre-shear point (σ_{SF}, τ_{SF}), Mohr semicircles analysis enables the determination of the following parameters (Fig. 1) [1–5]: the major principal stress (σ_1), the unconfined yield stress (f_c), the angle of internal friction (ϕ) and the angle of internal friction at steady state flow (ϕ_{SF}). The large Mohr semicircle is passing through the pre-shear

* Corresponding author.
E-mail address: guillaume.bernard-granger@cea.fr (G. Bernard-Granger).

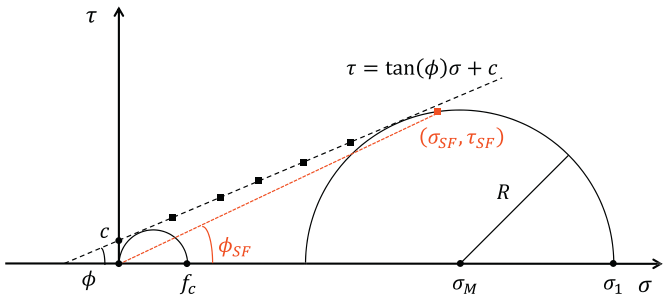

Fig. 1. Linear yield locus and Mohr semicircles analysis to determine key parameters from a shear test completed on a powdered or bulk material.

point (σ_{SF},τ_{SF}) and is tangent to the yield locus. The small Mohr semicircle is running through the origin and is tangent to the yield locus. According to Relation (1) and to Fig. 1, the static inter-particle friction coefficient and the angle of internal friction are linked by $\mu = \tan(\phi)$.

Using geometric considerations from Fig. 1, it is easy to show that [2]:

$$f_c = \frac{2c\cos(\phi)}{1-\sin(\phi)} \tag{2}$$

$$R = \sqrt{(\sigma_{SF}-\sigma_M)^2 + [\sigma_{SF}\tan(\phi_{SF})]^2} \tag{3}$$

$$\sin(\phi) = \frac{R}{\sigma_M + \frac{c}{\tan(\phi)}} \tag{4}$$

By combining Relations (3) and (4), solving the quadratic equation obtained and eliminating the solution that does not make physical sense (requirement for the large Mohr semicircle to be tangent to the yield locus at a point beyond its end point) leads to [2]:

$$\sigma_M = \tan^2(\phi)\sigma_{SF} + \tan(\phi)c + \sigma_{SF} - \frac{\sqrt{[\tan(\phi)\sigma_{SF}+c+\sigma_{SF}\tan(\phi_{SF})][\tan(\phi)\sigma_{SF}+c-\sigma_{SF}\tan(\phi_{SF})]}}{\cos(\phi)} \tag{5}$$

According to Fig. 1, the major principal stress at steady-state flow, σ_1 is then equal to [2]:

$$\sigma_1 = \sigma_M + R = \sigma_M + \sqrt{(\sigma_{SF}-\sigma_M)^2 + [\sigma_{SF}\tan(\phi)]^2} \tag{6}$$

with σ_M being representative of the center of the large Mohr semicircle.

To be able to classify the flow behavior of powders and bulk solids, Jenike proposed to use the flow index, ff_c, defined as the ratio of the major principal stress σ_1 to the unconfined yield stress f_c [6]:

$$ff_c = \frac{\sigma_1}{f_c} \tag{7}$$

Then a classification of the flow behavior of powdered materials and bulk solids has been proposed regarding the value of the ff_c parameter [6,7]:

- $ff_c < 1$ – Not flowing
- $1 < ff_c < 2$ – Very cohesive
- $2 < ff_c < 4$ – Cohesive
- $4 < ff_c < 10$ – Easy flowing
- $10 < ff_c$ – Free flowing.

For some industrial applications, the powdered material used to shape green pellets/tablets or to fill capsules is indeed a mixture of different raw powders. For example, in the nuclear industry, the MOX (Mixed OXide) fuel that may be used in pressurized water reactors (PWR) is a mix of UO_2 and PuO_2 powders, such a mixture being

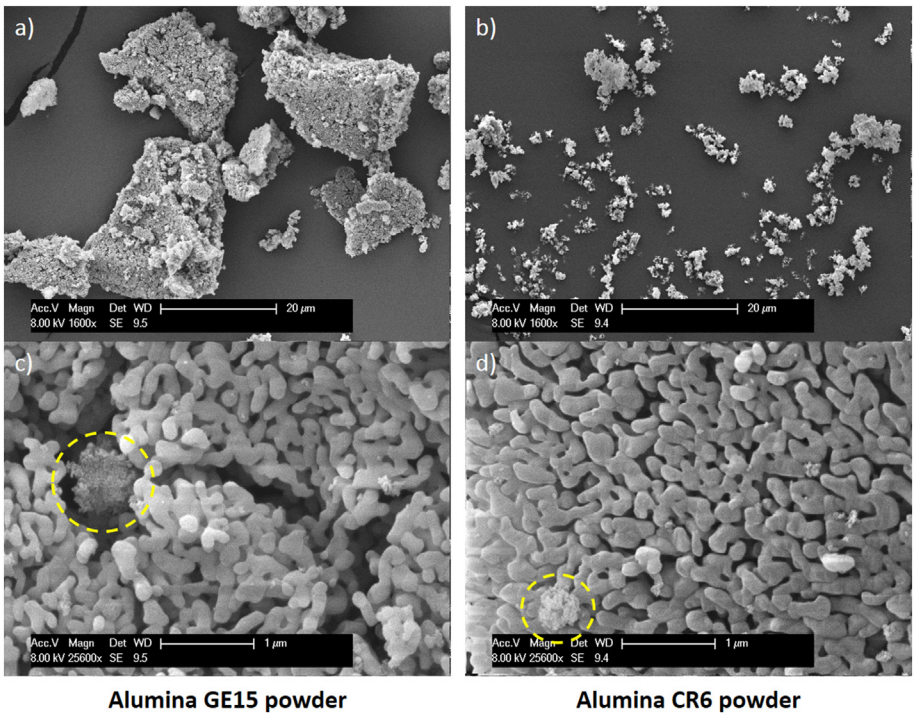

Fig. 2. SEM observations on the alumina raw powders; a) GE15 – General view; b) CR6 – General view; c) GE15 – Details at higher magnification; d) CR6 – Details at a higher magnification. The yellow doted-ellipses underline the presence of a minor phase. (For interpretation of the references to colour in this figure legend, the reader is referred to the web version of this article.)

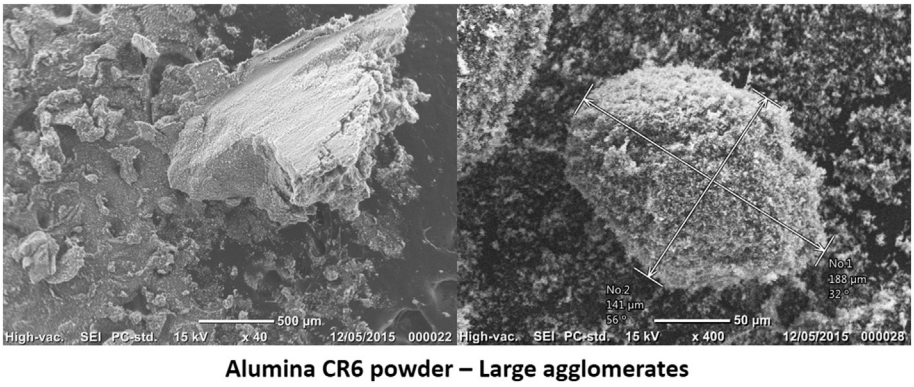

Fig. 3. SEM observations of typical large agglomerates present in the CR6 alumina raw powder.

elaborated using a dry route by a powder metallurgy process [8,29]. In the pharmaceutical industry, drug tablets and capsules are made/filled with a mixture of powdered active pharmaceutical ingredients (API) and excipients. Then, the flow properties of such nuclear or pharmaceutical mixtures are possibly a function of the contents of each individual powdered constituent, as investigated recently by Capece for pharmaceutical formulations [9,10].

Accordingly, the present paper focuses on investigating the flow properties of binary mixtures of alumina powders using shear tests. The influences of the mixing and environmental conditions are addressed. The contributions of the Van der Waals, capillary, electrostatic and gravitational forces are discussed.

2. Material and methods

2.1. Powders

The CR6 and GE15 (Baikowski, La-Balme-de-Sillingy, France) alumina powders have been selected for the investigations.

X-ray diffraction (XRD, Cu-K_α radiation with $\lambda = 1.5406$ Å, D5000, Bruker AXS SAS, Champs-sur-Marne, France) shows that both powders exhibit only peaks matching with the α-alumina species (trigonal structure, space group R3C, lattice parameters are a = 4.750 Å and c = 12.982 Å, theoretical density of 3.987 g/cm^3, JCPDS reference file 46-1212). The powder manufacturer certifies that the CR6 and GE15 powders are respectively made of 100 and 90% of the α-alumina species [11]. It probably signifies that 10% of the mater constituting the GE15 powder is made of an amorphous or a transition alumina because no specific peak does appear on X-ray diffractograms, the resolution limit for oxide-based materials being in the range 5-10%.

The specific surface area (SSA^{BET}) of both powders has been measured using the Brunauer-Emmett-Teller method (BET, 3Flex, Micromeritics France S.A.R.L., France, gaseous nitrogen is the adsorbate, two measures for each powder, multi-points method). The obtained values are 15.5 ± 0.5 and 6.6 ± 0.5 m^2/g for the GE15 and CR6 powders, respectively. Using the SSA^{BET} values, an equivalent crystallite diameter is calculated for each powder using the following expression (crystallites are assimilated to perfectly dense spheres devoted of any closed porosity, a monodisperse size distribution of the crystallites is assumed) [12]:

$$d_{BET} = \frac{6}{\rho_{th} SSA^{BET}} \tag{8}$$

with ρ_{th} the theoretical density of the alumina α-species (3.987 g/cm^3). Accordingly, the equivalent crystallite diameter is calculated to be around 100 nm and 230 nm for the GE15 and CR6 powders, respectively.

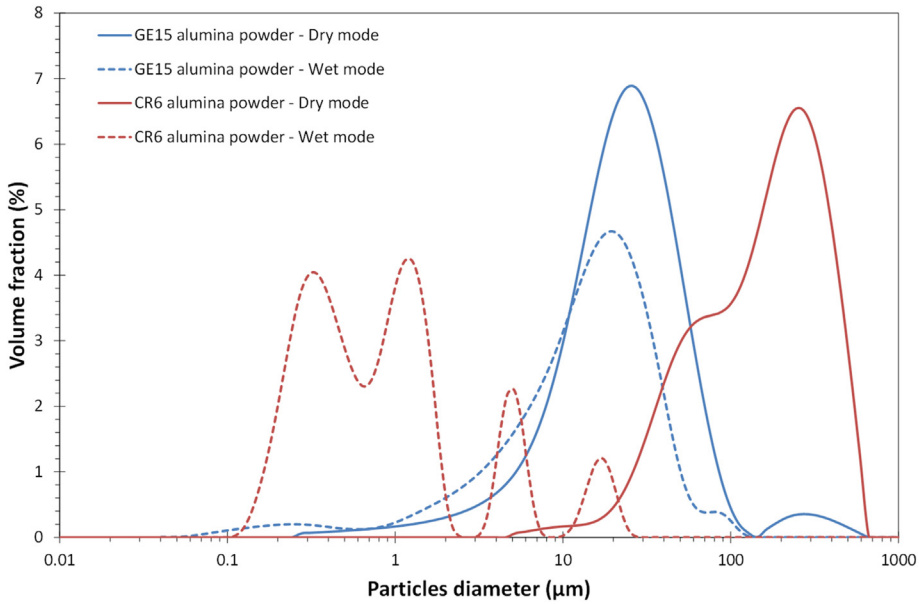

Fig. 4. Particle size distribution measured by laser diffraction for the GE15 and CR6 alumina raw powders. Solid lines are obtained in dry mode. Dotted lines are obtained in wet mode.

Table 1
Key properties measured on the GE15 and CR6 alumina powders.

Property	GE15 alumina powder	CR6 alumina powder
Crystalline structure	90% a	100% a
BET specific surface area (m^2/g)	15.5	6.6
BET crystallite equivalent diameter (nm)	100	230
Morphology	Tabular, angular	Random
Key parameters of the volume distribution size using laser particle size analyzer in dry configuration (0.1 bar)	$D_{32} \approx 12$ μm $D_{43} \approx 37$ μm $d_{10} \approx 8$ μm $d_{50} \approx 25$ μm $d_{90} \approx 62$ μm *Mode* ≈ 27 μm	$D_{32} \approx 98$ μm $D_{43} \approx 210$ μm $d_{10} \approx 45$ μm $d_{50} \approx 183$ μm $d_{90} \approx 426$ μm *Mode* ≈ 271 μm
Freely settled density (g/cm^3)	0.38	0.88
Tapped density (g/cm^3) – 2400 counts	0.57	1.24
Carr index	33	29
Hausner ratio	1.49	1.41
Porous degree of the freely settled powder bed (%)	90	78
Humidity level – As released from container (wt%)	0.42	0.31

The morphology of both powders has been observed using scanning electron microscopy (SEM, Philips XL30 ESEM FEG, FEI France, Mérignac, France, some powder is set on a carbon scotch with a slight platinum metallization) in secondary electron mode (acceleration voltage set in the range 8-15 kV). Fig. 2 shows the typical aspect of both powders at different magnifications. The GE15 powder is made of particles of tabular/angular shape (Fig. 2a). Their size varies from a few microns to a few tens of microns. In comparison, the CR6 powder is made of much finer particles of random shape (Fig. 2b). The CR6 powder has a strong tendency to form large agglomerates (Fig. 3) and it is indeed very difficult to find areas where elemental particles are identified, as it is the case on Fig. 2b. Such large agglomerates have an average diameter running from several tenths of micrometers to several hundreds of micrometers. Looking at the surface of the particles constituting the GE15 powder (Fig. 2c) shows that they are constituted by an aggregation of much finer entities, having a broadly rounded shape morphology and an average equivalent diameter around 200 nm (image analysis on 50 entities, Image J free software, developed by the National Institute of Health, USA). Some solid necks are also joining such entities. Similar observations on the surface of the particles constituting the CR6 powder show that they are also made of an aggregation of fine entities, but these entities have now a more vermicular shape, are larger with an average equivalent diameter around 280 nm and neck bonding is now generalized (Fig. 2d). It has to be outlined that a second phase is located in the particles constituting the GE15 and CR6 powders. It looks like spherical hanks, having a submicron diameter, that are made of an aggregation of nanometer-sized individual entities (yellow dotted-circles on Fig. 2c and d). The concentration of such spherical hanks is much higher in the GE15 powder. Consequently, such hanks are possibly made of amorphous or transition alumina. Then it can be postulated that the CR6 powder is probably obtained by a calcination treatment of the GE15 one followed by a grinding step. Accordingly, in comparison to the GE15 powder, the particles constituting the CR6 one are finer with a random shape, the elemental entities constituting the particles are larger with a vermicular shape (numerous bonding necks are also present linking the entities) and the amount of spherical hanks made of amorphous or transition alumina is strongly reduced. Such a scenario is supported by the results obtained from XRD experiments, specific surface area measurements and SEM observations.

The volume size distributions of the GE15 and CR6 powders have been determined using LASER diffraction (Mastersizer 3000, Malvern Instruments, Malvern, UK, LASER wavelength of 633 nm, Mie configuration, real part of the alumina refractive index set to 1.766, imaginary part of the alumina refractive index set to 0.010) in dry mode (Aeros S dry powder disperser, straight venturi), with dispersion overpressure set to 0.1 bar to minimize as much as possible powder destructuring during the measurements. Fig. 4 shows the volume size distributions of the GE15 and CR6 alumina powders. The associated characteristic

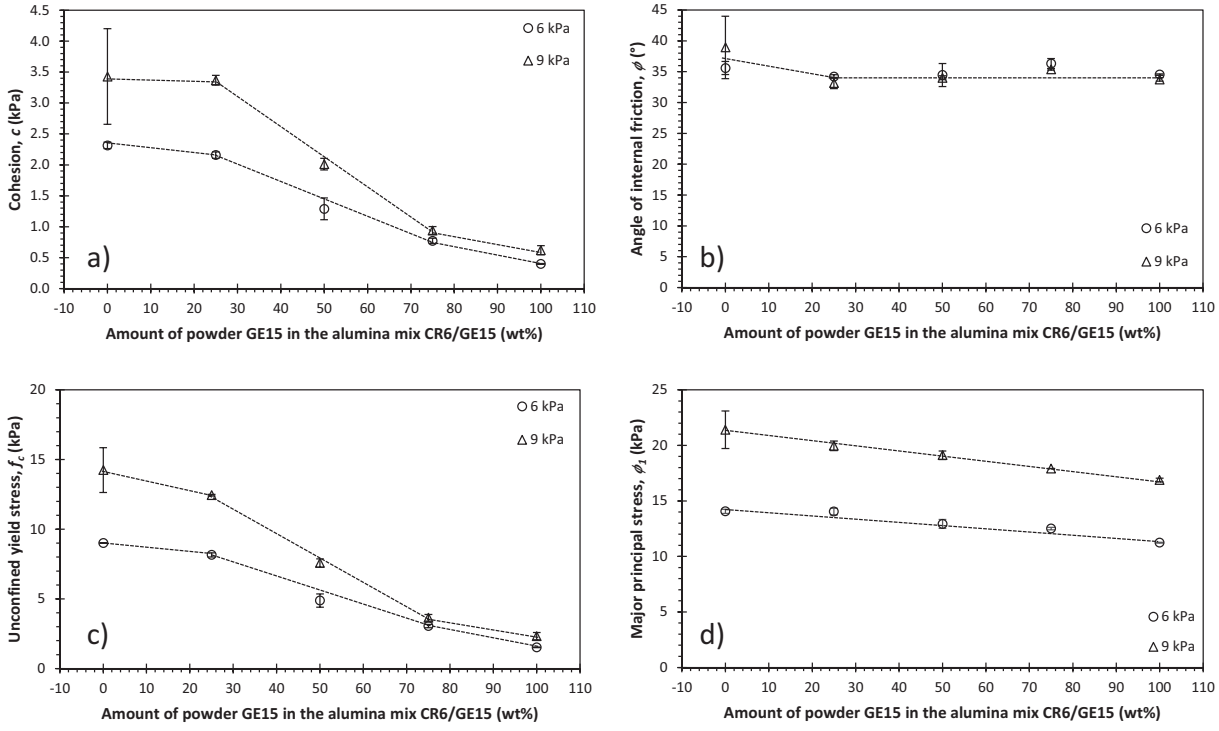

Fig. 5. Evolution of the key parameters extracted from the shear tests as a function of the composition of the alumina-based powder mixtures investigated; a) Cohesion; b) Angle of internal friction; c) Unconfined yield stress; d) Major principal stress. Two values have been retained for the pre-shear consolidation stress: 6 and 9 kPa.

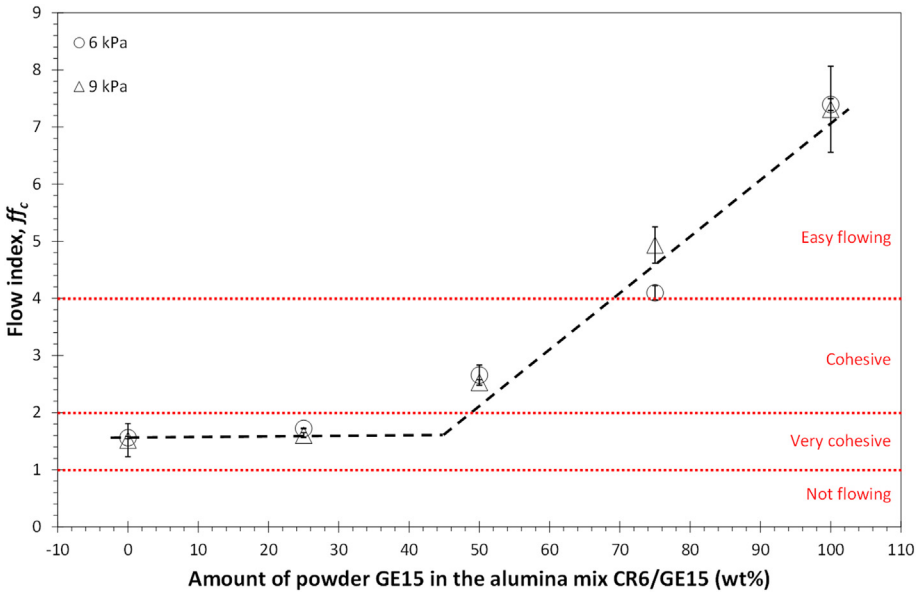

Fig. 6. Evolution of the flow index as a function of the composition of the alumina-based powder mixtures investigated. Two values have been retained for the pre-shear consolidation stress: 6 and 9 kPa.

size-parameters are summarized in Table 1. The size distribution is close to be monomodal for the GE15 powder. In comparison, it is clearly bimodal for the CR6 one. Moreover all the distribution related to the CR6 powder is shifted towards higher diameters. Additional LASER diffraction experiments have also been completed using a wet configuration (LS 13320, Beckman Coulter, Beckman Coulter France, Villepinte, F, multi-wave length configuration, Mie configuration, real and imaginary parts of the alumina refractive index are set to the adequate values for the different wavelengths used) where both powders are dispersed in deionized water for the measurements with an ultrasounds application. The results are also shown on Fig. 4. For information, averaged particles diameter (d_{50}) in wet mode are 0.8 and 15 μm for the CR6 and GE15 powders, respectively. Then it is confirmed that the CR6 alumina powder is much more sensitive to agglomeration in air than the GE15 one.

The freely settled and tapped densities have been measured for both powders using a powder volumenometer (STAV 2003, J. Englesmann AG, Ludwigshafen, D, glass test tube volume fixed to 100 cm^3, tapping number fixed to 2400). The freely settled (*FSD*) and tapped densities (*TD*) are 0.38 ± 0.04 and 0.57 ± 0.03 g/cm^3 against 0.88 ± 0.03 and

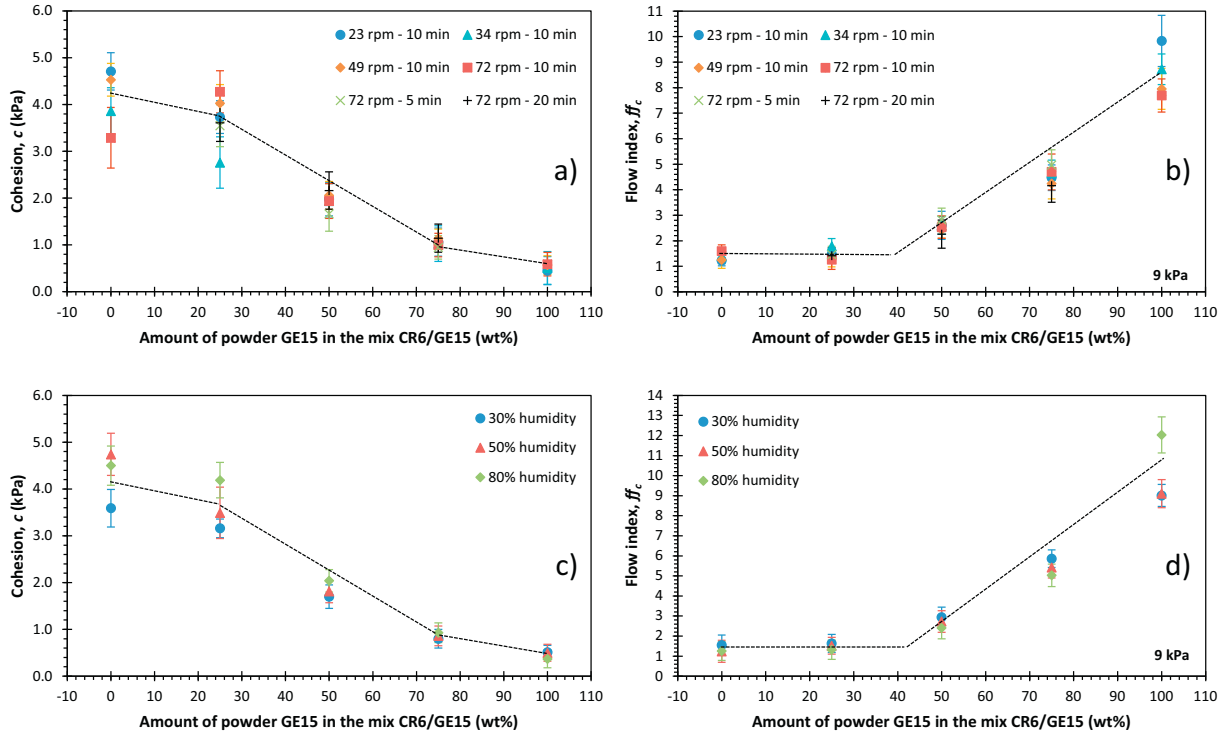

Fig. 7. Influence of the mixing parameters and of the relative humidity level used to precondition the powder bed on the key parameters extracted from the shear tests as a function of the composition of the alumina-based powder mixtures investigated; a) Mixing conditions – Cohesion; b) Mixing conditions – Flow index; c) Relative humidity – Cohesion; d) Relative humidity – Flow index. The pre-shear consolidation stress is fixed to 9 kPa.

Table 2
Influence of preconditioning conditions on the humidity level adsorbed by the GE15 and CR6 alumina raw powders.

Relative humidity (%)	30	50	80	Exiting from the container
GE15 – Humidity content (wt%)	0.52 ± 0.03	0.63 ± 0.04	0.77 ± 0.04	0.42 ± 0.02
CR6 – Humidity content (wt%)	0.29 ± 0.03	0.26 ± 0.03	0.40 ± 0.02	0.31 ± 0.03

1.24 ± 0.02 g/cm^3 for the GE15 and CR6 powders, respectively (three measurements for each type of density). Accordingly, for each powder the Carr index, I_{Carr}, and the Hausner ratio, R_H, are calculated using the following expressions [13]:

$$I_{Carr} = \left(\frac{TD - FSD}{TD}\right) \times 100 \quad (9)$$

$$R_H = \frac{TD}{FSD} \quad (10)$$

Then typical values of Carr index and Hausner ratio are found to be 33 ± 1 and 1.49 ± 0.02 for the GE15 powder against 29 ± 1 and 1.41 ± 0.02 for the CR6 one. Such values are typical of powders having a poor or even very poor aptitude to freely settle [14].

Using a mixing rule, it is easy to calculate the porous degree, ε, of the freely settled powder bed for each powder (interparticle and intraparticle porosities are taken into account):

$$\varepsilon = \frac{FST - \rho_{th}}{\rho_{air} - \rho_{th}} \quad (11)$$

where ρ_{air} is the density of air at room temperature (around 1.2x10^{-3} g/cm^3) and the other parameters have been already defined before. Then ε values are calculated to be around 90% and 78% for the GE15 and CR6 alumina powders, respectively.

The humidity level of both powders as-released from their own container has been measured using a thermo-balance (KERN MRS 120-3, Kern & Sohn GmbH, Balingen-Frommern, D, temperature fixed to 105 °C, soak at 105 °C set to 20 min, two measurements for each powder). Values of 0.42 ± 0.02 and 0.31 ± 0.03 wt% have been obtained for the GE15 and CR6 powders, respectively (the humidity level is calculated by dividing the absolute value of the weight loss by the initial mass of powder introduced in the thermo-balance, assuming that only water is removed).

Finally, the different properties of the GE15 and CR6 alumina powders have been summarized in Table 1.

2.2. Elaboration of powder mixtures

Different CR6/GE15 alumina powder mixtures compositions have been retained: 100CR6/0GE15, 75CR6/25GE15, 50CR6/50GE15, 25CR6/75GE15 and 0CR6/100GE15, the different numbers being the mass fraction of each powder.

A cylindrical polyethylene jar of 500 cm^3 volume is filled, at room temperature and in the lab atmosphere, with the adequate weight of each powder just exiting from the containers, the filling ratio being fixed to 50%. The jar is then mounted on a mixing equipment adopting an oscillation-rotation movement (Turbula® T2C, Glenn Mills, Clifton, USA). In a first step, the experiments have been conducted using a mixing time fixed to 10 min and a stirring rate fixed to 22 revolution-per-minute (rpm). Such parameters have been already proved to be relevant to prepare homogeneous mixtures made of cohesive powders using the same equipment [30]. Additional tests have been also completed using different mixing times (5 and 20 min) and stirring rates (34, 49 and 72 rpm). Indeed, from an industrial point of view, it is important to know which the most effective operating conditions are allowing to obtain a mixture in the shortest possible time.

At the end of the mixture step, samples of the collected powdered media are then directly characterized using shear tests or conditioned during 48 hours in a climatic chamber (WKL 34/10, Weiss Teknik France, Cergy Pontoise, F), enabling a strict control of the temperature and humidity, before the shear tests. From an industrial point of view it is also critical to know if powder mixtures are sensitive to moisture uptake during storage, as this can have a strong influence on flowability and, for example, shaping by automatic uniaxial pressing.

2.3. Shear tests

Shear tests have been performed on the different powder mixtures and also for different conditions of realization of the mixtures and different conditioning conditions of the mixtures elaborated. A powder rheometer (FT4, Freeman Technology, Tewkesbury, UK) equipped with a 10 cm^3 borosilicate glass shear cell has been used. Duplicate measurements for each powder bed to be evaluated were conducted for a pre-shear consolidation stress value, σ_{SF}, fixed to 6 and 9 kPa (some tests were conducted at 9 kPa only), thought to be representative of the

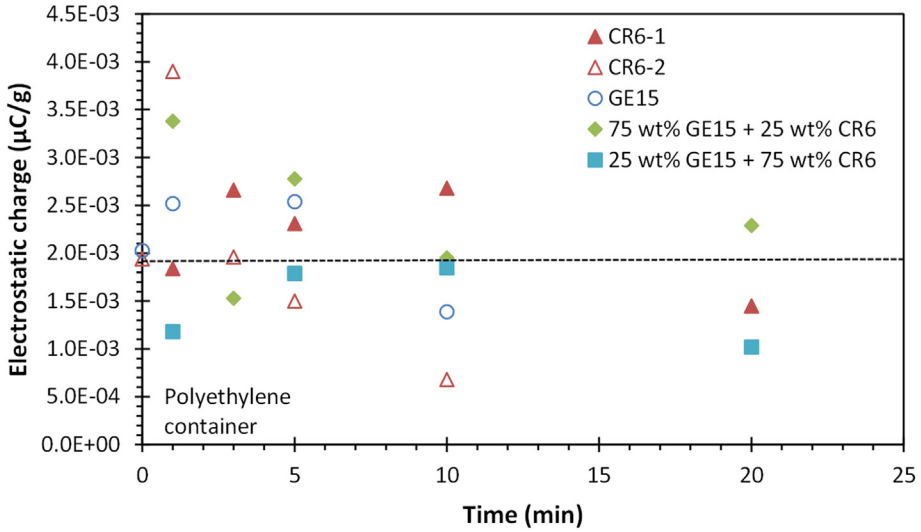

Fig. 8. Evolution of the electrostatic charge as a function of time for the GE15 and CR6 alumina powders and two mixtures compositions.

pressure range encountered by a powder when stocked at the bottom of hoppers before being shaped by uniaxial dry pressing. A linearized yield locus is then generated with five sets of (σ,τ) data points at incipient flow, the σ values being in the range $0.2\sigma_{SF}$-$0.9\sigma_{SF}$, as generally recommended [15]. For each parameter extracted from the Mohr semicircle analysis, a mean value and standard deviation (sd) are then calculated (the error bars that will be visible in the different figures are representative of $\pm sd$).

3. Results and discussion

3.1. Experimental results

On Fig. 5 are summarized the main results from the shear tests completed on the different powder mixtures.

Fig. 5a shows the evolution of the cohesion, c, as a function of the amount of powder GE15 introduced in the alumina mix CR6/GE15. It appears that the CR6 powder has a cohesive nature, with cohesion values in the range 2.5-3.5 kPa, depending on the pre-shear consolidation stress value retained. The higher the pre-shear consolidation stress value, the higher the cohesion. For comparison, the GE15 powder is almost non-cohesive, the cohesion value ranging from 0.4 to 0.6 kPa and being only slightly dependent on the pre-shear consolidation stress value. Concerning the cohesion of the different mixtures investigated, it appears that three different regimes exist whatever the pre-shear consolidation stress value adopted. For GE15 concentrations ranging from 0 to 25 wt%, the cohesion of the mix remains almost constant and significant. In that case the cohesion of the mix is governed by the CR6 powder. For GE15 concentrations ranging from 25 to 75 wt%, the cohesion of the mix decreases linearly with the increase of the GE15 concentration. Finally, for GE15 concentrations ranging from 75 to 100 wt%, the cohesion of the mix decreases slowly with the increase of the GE15 content. In that case the cohesion of the mix is governed by the GE15 powder. As already reported by Legoix [31], it is interesting to point out that a threshold concentration of the minority powder present in the mix may exist. Below this threshold value, the cohesion of the mix does not depend significantly on the content of the minority powder incorporated.

Fig. 5b shows the variation of the angle of internal friction, ϕ, as a function of the powder mixture composition. Whatever the pre-shear consolidation stress value retained, the GE15 and CR6 alumina raw powders exhibit similar ϕ values in the range 34-38°, leading to static inter-particle friction coefficients around 0.7-0.8. It also appears that ϕ is almost insensitive to the mixture composition and to the pre-shear consolidation stress value adopted.

On Fig. 5c is shown the variation of the unconfined yield stress as a function of the amount of powder GE15 introduced in the alumina mix CR6/GE15. The same trends as the ones reported just before for the evolution of the cohesion as a function of the powder mixture composition are observed. This is a normal result. Indeed the unconfined yield stress is a linear function of the cohesion, as shown by Eq. (2). Moreover, the angle of internal friction ϕ, also involved in Eq. (2), has been shown to be constant whatever the mix composition and the pre-shear consolidation stress used. Then cohesion and unconfined yield stress are varying in a similar way as a function of the powder mixture composition.

Fig. 5d shows the variation of the major principal stress at steady-state flow, σ_1, as a function of the powder mixture composition. The higher the pre-shear consolidation stress value, the higher the major principal stress at steady-state flow. Whatever the pre-shear consolidation stress value, the major principal stress at steady-state flow decreases linearly with the increase of the GE15 powder concentration in the mixture.

It is now possible to calculate the flow index, ff_c, for the different powder mixtures investigated according to Eq. (7). The result is shown on Fig. 6. Several observations can be made:

- All the points form a single curve whatever the pre-shear consolidation stress value adopted.
- The CR6 powder belongs to the "very cohesive" domain. For comparison, the GE15 powder belongs to the "easy flowing" one. It has to be recalled that both powders exhibited Carr index and Hausner ratio values typical of a poor or even very poor aptitude to freely settling. Accordingly, a given powder may exhibit completely different flow properties depending on its solicitation mode. The GE15 alumina powder has been shown to exhibit a tabular morphology. It is reasonable to imagine that such a morphology is unfavorable for free-settling properties. On the contrary, when flow properties are measured using shear experiments, a uniaxial consolidation stress is applied on the powder bed. Then the tabular morphology may be favorable for particles rearrangement and glide under stress, promoting a much easier flow when solicited under shear.
- It exists a threshold concentration of GE15 powder, C^*_{GE15}, below which the flow properties of the mixtures are always governed by the poor flow properties of the CR6 powder. According to Fig. 6, C^*_{GE15} is estimated to be in the range 30–45 wt%. For concentrations of GE15 above C^*_{GE15}, the flow index increases linearly with the increase in GE15 content introduced in the mixtures.
- Based on the dotted-lines interpolating the experimental points, it appears that adding a small amount of a "poor flowing" powder (CR6) into a mixture mostly based on a "good flowing" powder (GE15) is strongly detrimental to the flow properties of the mixture. Conversely, adding a large amount (up to around 40 wt%) of a "good flowing" powder (GE15) into a mixture mostly based on a "poor flowing" powder (CR6) keeps the flow properties of the mixture to a poor level.

The influence of mixing time and speed on the cohesion and flow index of alumina-based CR6/GE15 powder mixtures have been investigated. For a pre-shear consolidation stress value fixed to 9 kPa, Fig. 7a and b show that unique behaviors regarding the variations of the cohesion and flow index as a function of the mixture composition are observed. Let's take a closer look at the conditions of preparation of the mixtures used. By multiplying the stirring speed of the Turbula® by the stirring time, the total number of stirring revolutions of the formulations is obtained. Taking into account the mixture parameters given in Fig. 7a and b, this number lays between 230 and 1440 revolutions. There is therefore a difference of a factor equal to about 525% between the most stirred and the least stirred mixture, from this point of view. By not taking into account the oscillating motion of the Turbula® and taking into account only its rotational movement, one can get a rough idea of the kinetic energy applied to the mixing system. The kinetic energy, E_c, of an object in rotation is given by [16]:

$$E_c = \frac{1}{2} J\omega^2 \tag{12}$$

with: J the moment of inertia of the polyethylene cylinder containing the powders to be mixed and ω the speed of rotation applied by the mixer. Consider that the maximum kinetic energy applied to the cylindrical container, E_m, is obtained for the maximum speed of rotation, ω_m, equal to 72 rpm. It is then easy to show that the kinetic energy, E_i, applied to the cylindrical container is connected to E_m by means of the following expression:

$$E_i = \left(\frac{\omega_i}{\omega_m}\right)^2 E_m \tag{13}$$

For the rotational speeds of the mixing system fixed at 22, 34 and 49 rpm, we thus achieve mixing kinetic energies respectively equal to $0.09E_m$, $0.22E_m$ and $0.46E_m$. It thus appears in the end that, despite the rather drastically different mixing conditions (total number of

revolutions and approximate kinetic energy), these have no significant influence on the rheological properties of the powder mixtures investigated.

Additional tests (pre-shear consolidation stress value fixed to 9 kPa) have been completed on powder mixtures conditioned under different relative humidity levels fixed to 30, 50 and 80% before shearing. Fig. 7c and d show that unique behaviors regarding the variations of the cohesion and flow index as a function of the mixture composition are observed. At the same time the capacities of the CR6 and GE15 powders to adsorb humidity have been investigated using thermo-balance measurements, the results being summarized in Table 2. If for the CR6 powder, the relative maximum moisture recovery is only 33%, while it reaches 83% for the GE15 powder. A variation of moisture in alumina-based powders of these orders of magnitude is known, to have a detrimental effect on the ability of the powders to be shaped by high speed uniaxial pressing (sticking to the compaction punches, for example) [17,18]. These relative humidity variations in the CR6 and G15 powders are therefore considered as significant. Then, despite a significant moisture uptake of the CR6 and GE15 powders, it has no influence on the rheological properties of the powder mixtures investigated. Nonetheless, it has to be underlined that both powders contain a significant amount of adsorbed moisture just exiting from their storage containers. Therefore, there is probably a critical moisture content beyond which no influence is found on the rheological properties of the two powders and different mixtures investigated. It is possible that the moisture content of the GE15 and CR6 powders exiting from the storage container is already higher than this critical content. It would be very helpful in the future to complete additional experiments with perfectly dried GE15 and CR6 powders to ascertain the existence of such a critical moisture content.

3.2. Theoretical developments

Let us now discuss about the different interaction forces possibly involved in the rheological behavior of the CR6/GE15 powder mixtures investigated.

First consider the electrostatic forces. If interactions are coulombic, the electrostatic force absolute value between two smooth charged spherical particles is simply given by:

$$|F_{ES}| = \frac{\pi D_1^2 D_2^2 C_1 C_2}{4\varepsilon\varepsilon_0 \lambda^2} \tag{14}$$

where: D_1 / D_2 and C_1 / C_2 are, respectively, the diameters and surface charges of both particles in interaction, ε is the relative dielectric constant of the medium where the interaction occurs, ε_0 is the vacuum dielectric constant (8.90×10^{-12} $C^2.N^{-1}.m^{-2}$) and λ is the distance between the centers of both particles.

The maximum electrostatic interaction force is given for $\lambda = R_1 + R_2 = \frac{D_1+D_2}{2}$ (the two charged particles are tangent). Then Eq. (14) changes to:

$$|F_{ES}|^{max} = \frac{\pi C_1 C_2}{\varepsilon\varepsilon_0}\left(\frac{D_1 D_2}{D_1 + D_2}\right)^2 \tag{15}$$

The electrostatic charge that may develop at the surface of the GE15 and CR6 alumina powders during the mixing experiments have been addressed. The powder is first introduced into a polyethylene cup (same material as the one used for the mixture experiments) which is then placed in a rotating machine positioned in a glovebox where the relative humidity level is fixed to 50%. This allows the powder to be electrostatically charged by rubbing on the cup walls (triboelectrification). The charge developed is then measured by pouring the cup powder into a Faraday cage container connected to a multimeter (in-house developments). Charge kinetics is thus produced by varying the stirring time. This kind of experiment gives a global and non-local information about the charge of the powder. The charge is given per unit mass of powder, which is weighed beforehand.

Fig. 8 shows the variation of the electrostatic charge that develops for the CR6 and GE15 powders and two mixture compositions of both (only one measurement for each condition, except for the CR6 raw powder were two measurements have been completed and reported. At this stage, it can be noted that the two measurements made on the CR6 powder give fairly similar results although the low reproducibility of electrostatic charges measurements is very common.). Whatever the powder bed composition and the stirring time, an average electrostatic charge around 2.0×10^{-3} μC/g is retained (black dotted line in Figure 8). The specific surface areas of the CR6 and GE15 powders are respectively 6.6 and 15.5 m^2/g (Table 1). From these data, the surface charge per unit area values are calculated to be 3.0×10^{-4} μC/m^2 and 1.3×10^{-4} μC/m^2 for the CR6 and GE15 powders respectively. Assuming a particle diameter of 15 and 0.8 μm for the GE15 and CR6 powder, respectively and considering that the interaction medium is air (ε~1), the electrostatic interaction force is calculated to be 3.4×10^{-19} N between two GE15 particles, 5.1×10^{-21} N between two CR6 particles and 7.9×10^{-21} N between one GE15 particle and one CR6 particle.

Consider now the capillary force between two smooth spherical particles of radii R_1 and R_2 connected by a water meniscus defined by its radii of curvature r_n and r_p and by the filling angles β_1 and β_2, as shown on Fig. 9. The contact angles of the water meniscus towards the surface of both particles are referred as θ_1 and θ_2.The separation distance between the surface of both particles is referred as d. From Fig. 9, straightforward geometrical considerations show that [19,20]:

$$r_n = R_1\ \sin(\beta_1) - r_p[1 - \sin(\beta_1 + \theta_1)] \tag{16}$$

$$r_p = \frac{R_1[1 - \cos(\beta_1)] + R_2[1 - \cos(\beta_2)] + d}{\cos(\beta_1 + \theta_1) + \cos(\beta_2 + \theta_2)} \tag{17}$$

$$\beta_1 = 2\ \arctan\left[\frac{A\ \sin\left(\frac{\beta_2}{2}\right) + B\ \cos\left(\frac{\beta_2}{2}\right)}{C\ \cos\left(\frac{\beta_2}{2}\right) - D\ \sin\left(\frac{\beta_2}{2}\right)}\right] \tag{18}$$

with:

$$A = (d + 2R_2)\ \cos\left(\frac{\theta_2 - \theta_1}{2}\right) \tag{19}$$

$$B = d\ \sin\left(\frac{\theta_2 - \theta_1}{2}\right) \tag{20}$$

$$C = (d + 2R_1)\ \cos\left(\frac{\theta_2 - \theta_1}{2}\right) \tag{21}$$

$$D = (d + 2R_1 + 2R_2)\ \sin\left(\frac{\theta_2 - \theta_1}{2}\right) \tag{22}$$

By taking into account the effects of surface tension and Laplace force because of curved interfaces, the capillary force at the neck represented by the contact radius AB (Fig. 9) is simply given by [19,21,22]:

$$F_c = \pi R_1 \gamma_{LV}\ \sin(\beta_1)\left[2\ \sin(\beta_1 + \theta_1) + R_1\ \sin(\beta_1)\left(\frac{1}{r_p} - \frac{1}{r_n}\right)\right] \tag{23}$$

where γ_{LV} is the surface tension of water (72.8 mN/m).

For contact angles θ_1 and θ_2 set to zero (a perfect wetting is assumed, in that case the capillary force calculated will be maximum), Fig. 10a shows the variation of the capillary force as a function of the filling angle β_2 for a water meniscus joining one particle of CR6 powder and one particle of GE15 powder (blue continuous line), two particles of CR6 powder (small red doted-line) and two particles of GE15 powder

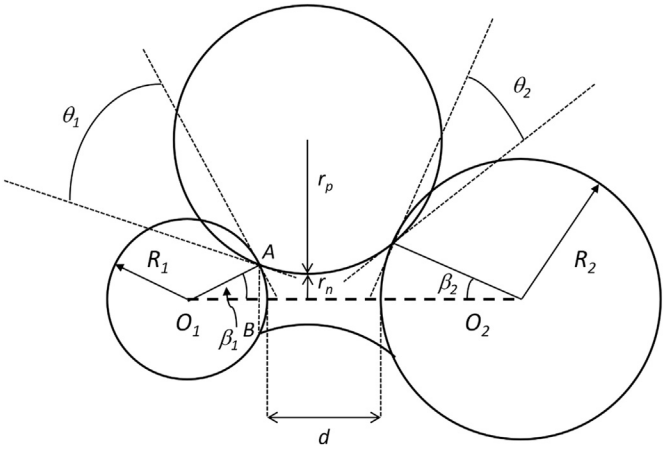

Fig. 9. Geometrical configuration used to investigate the capillary force between two solid spherical particles of diameter R_1 and R_2 separate by a distance d, joined by a water meniscus defined by its radii of curvature r_p and r_n, the filling angles β_1 and β_2 and the contact angles θ_1 and θ_2.

(large green doted-line) with the separation distance between particles, d, assumed to be around 4 Å (this value is representative of an average diameter for all atoms listed in the periodic table, it implies that only one atom/molecule can be positioned between two interacting objects) [23]. Whatever the configuration considered, the capillary force has a much higher intensity than the one calculated before for the electrostatic contribution.

Let's move on now on the Van der Waals interaction in air between two smooth alumina spherical particles of diameter D_1 and D_2 separated by a distance d (the distance between the surfaces of both spheres). The Van der Waals force is given by [23,24]:

$$F_{VDW} \approx \frac{[A_{Al2O3-Al2O3}]^{air}}{12d^2}\frac{D_1 D_2}{D_1 + D_2} \tag{24}$$

with $[A_{Al2O3-Al2O3}]^{air}$ the Hamaker constant. Using the Lifshitz theory [25] and the Tabor-Wintertorn approximation [26], the non-retarded Hamaker constant is given by [24]:

$$[A_{Al2O3-Al2O3}]^{air} \approx \frac{3}{4}kT\left(\frac{\varepsilon_1-\varepsilon_3}{\varepsilon_1+\varepsilon_3}\right)^2 + \frac{3h\nu_e}{16\sqrt{2}}\frac{\left(n_1^2-n_3^2\right)^2}{\left(n_1^2+n_3^2\right)^{\frac{3}{2}}} \tag{25}$$

where: T is the absolute temperature, k is the Boltzmann constant (1.38×10^{-23} J.K^{-1}), ε_1 is the static relative dielectric constant of alumina (~10.1 [27]), ε_3 is the static relative dielectric constant of the interaction media (i.e. air, ~1), h is the Planck constant (6.62×10^{-34} J.s), ν_e is the main frequency of electronic absorption positioned in the UV range (~3×10^{15} s^{-1}), n_1 is the alumina refractive index in the visible range (~1.76 for a wavelength of 600 nm [28], taking into account only the real-part of the refractive index and neglecting absorption because alumina is transparent in the visible range, as demonstrated by sapphire) and n_3 is the refractive index of the interacting medium in the visible range (i.e. air, ~1 for a wavelength of 600 nm). Accordingly, a value of $[A_{Al2O3-Al2O3}]^{air}$ around 14×10^{-20} J is calculated at room temperature.

Neglecting the contribution of the presence of a water meniscus (a more strict calculation taking into account this point is addressed in [21,22]), the Van der Waals forces between one particle of CR6 powder and one particle of GE15 powder, two particles of CR6 powder and two particles of GE15 powder have been calculated, always assuming a separation distance between particles, d, to be around 4 Å. Fig. 10b shows the results which are compared with the ones obtained for the capillary forces for the same interaction conditions and for a filling angle β_2 fixed to 2° (in that case the filling angle β_1 is around 35°, particle 1 is not submerged by water forming the meniscus, the contact angles θ_1 and θ_2 are set to zero). Whatever the interaction configuration, the capillary force is always higher than the Van der Waals one by a factor in the range 3-6. Nonetheless, if the electrostatic forces are much lower in magnitude and can be definitively neglected (see above) regarding a balance of forces, it is clearly not the case for the Van der Waals ones.

Capece has defined a granular Bond number (the ratio between the inter-particle cohesive forces to particle weight) for multi-component mixtures (i.e. powder blends) and used it to predict the flow index, ff_c, of binary, ternary and quaternary mixtures of pharmaceutical compounds [9,10]. The bond number of a powder mixture is given by [9]:

$$B_{mix} = \left(\sum_{i=1}^{N}\sum_{j=1}^{N}\frac{\omega_{ij}}{B_{ij}}\right)^{-1} \tag{26}$$

with i and j being indices representing each component, ω_{ij} acting as weighting functions and B_{ij} being the granular bond number between particles of type i and j. The bond number for particles i and j in interaction is simply given by:

$$B_{ij} = \frac{F_{ij}}{W_{ij}} \tag{27}$$

where F_{ij} is the total interaction force between both particles considered, then, in our case, typically the sum of the Van der Waals and capillary actions neglecting the electrostatic one, and W_{ij} is the particle weight contribution.

Capece assumed a harmonic mean to define the particle weight contribution [9]:

$$W_{ij} = \frac{2W_i W_j}{W_i + W_j} \tag{28}$$

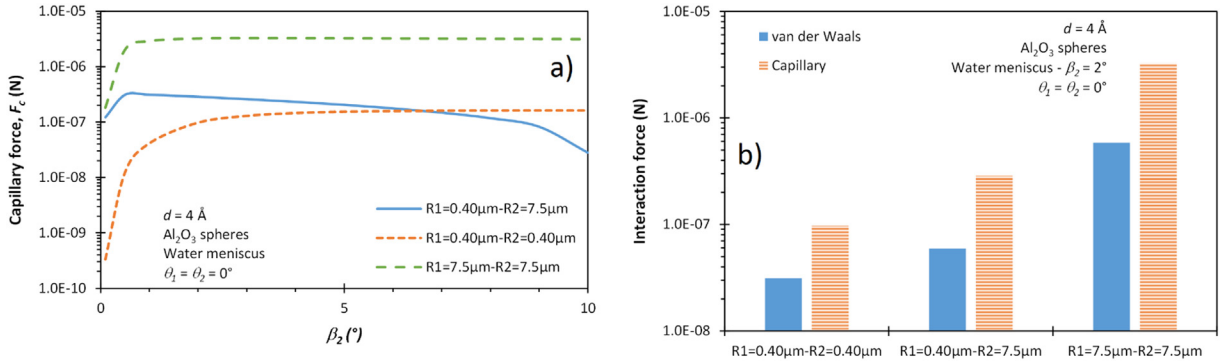

Fig. 10. Inter-particle forces; a) Capillary force for different geometrical configurations; b) Comparison between the Van der Waals and capillary forces for different geometrical configurations.

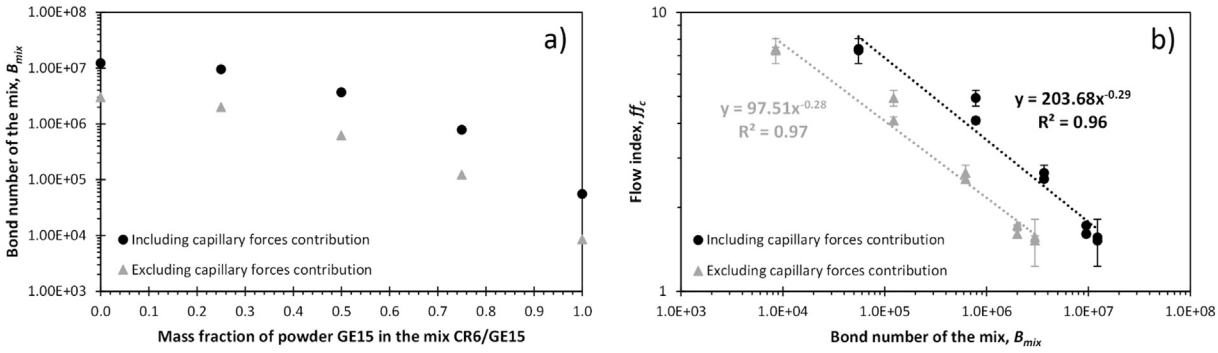

Fig. 11. a) Evolution of the Bond number of the mix as a function of the composition of the alumina-based powder mixture; b) Evolution of the flow index as a function of the Bond number of the alumina-based powder mixtures.

with W_i and W_j the weight of the particles i and j, respectively. Considering that the particles are smooth spheres with diameters D_i and D_j and densities ρ_i and ρ_j, straightforward calculations show that the particle weight contribution is given by:

$$W_{ij} = \frac{\pi \rho_i \rho_j g}{3} \frac{D_i^3 D_j^3}{\rho_i D_i^3 + \rho_j D_j^3} \tag{29}$$

where g is the standard gravity value (~9.81 m.s^{-2}). For particles i and j made of the same material ($\rho_i = \rho_j$), Relation (29) becomes:

$$W_{ij} = \frac{\pi \rho_i g}{3} \frac{D_i^3 D_j^3}{D_i^3 + D_j^3} \tag{30}$$

For the weighting functions, Capece used the product of two material's fractional surface area $f_{i,j}^{SA}$ which gives the probability that these two materials come into contact. Then [9]:

$$\omega_{ij} = f_i^{SA} f_j^{SA} \tag{31}$$

For a mixture of two powders referred as *1* and *2* and taking into account that $\omega_{12} = \omega_{21}$ and $B_{12} = B_{21}$, it comes:

$$B_{mix} = \left[\frac{\left(f_1^{SA}\right)^2}{B_{11}} + \frac{\left(f_2^{SA}\right)^2}{B_{22}} + \frac{2 f_1^{SA} f_2^{SA}}{B_{12}} \right]^{-1} \tag{32}$$

where $f_2^{SA} = 1 - f_1^{SA}$ for a binary mixture.

Knowing the particle diameter (15 μm and 0.8 μm for GE15 and CR6, respectively) and the tapped density (0.57 g/cm^3 and 1.24 g/cm^3 for GE15 and CR6, respectively) for each powder, it is easy to calculate the fractional surface area parameters f_1^{SA} and f_2^{SA} for a given mixture composition. In a first step, the volume of each powder in a mixture of a given composition is calculated, considering an arbitrary total mass of 100 grams. The volume for one particle (assumed to be a sphere) for each powder is also calculated. Then it is possible to obtain the number of each particles in the powder mixture based on the arbitrary quantity of 100 grams. Calculating the surface for one particle (assumed to be a sphere) of each powder enables then to calculate the surface developed by all the particles of each powder involved in the mixture composition, having an arbitrary total mass of 100 grams. Then, it is easy to calculate the f_1^{SA} and f_2^{SA} values. The value of the tapped densities are retained for both powders because they appear more representative of the configuration of the powders during the realization of the mixtures.

Then, applying Relation (31) to the different GE15 / CR6 alumina powder mixtures investigated (the specific surface area values for both powders are summarized in Table 1, particle diameters of 15 and 0.8 μm are assumed as before for the GE15 and CR6 powders respectively, the density of alumina is assumed to be 3.98 g/cm^3, the Van der Waals and capillary inter-particle forces are the ones calculated before for the different configurations assumed) enables to calculate the bond number of the mixture, B_{mix}, as a function of the mass fraction of powder GE15 incorporated, as shown on Fig. 11a. On Fig. 11a is also shown the calculation done by neglecting the contribution of the capillary forces. In both cases, the Bond number decreases continuously with the increase of the mass fraction of powder GE15 incorporated in the mixture. Fig. 11b shows the variation of the flow index, ff_c, of the different powder mixtures as a function of B_{mix} for pre-shear consolidation stresses fixed to 6 and 9 kPa. As before, calculations were made taking into account and neglecting the contribution of capillary forces. In both cases, the flow index decreases continuously with the increase in B_{mix} and a power law relationship is empirically established between both parameters:

$$ff_c \approx 204 (B_{mix})^{-0.29} \tag{33}$$

taking into account the capillary forces contribution

$$ff_c \approx 98 (B_{mix})^{-0.28} \tag{34}$$

neglecting the contribution of the capillary forces

Such a power law expression linking ff_c and B_{mix} has been already reported by Capece who investigated the rheological properties of binary mixtures of pharmaceutical compounds [9]. Furthermore, it has to be outlined that Capece obtained and exponent of −0.27 [9] which is similar to the ones we got.

At this stage, it should be also noted that certain powdered mixtures investigated have good flow properties associated with a relatively high bond number (greater than 1000). This result is substantially different from what has been reported by Capece [9]. In his case, ff_c values comparable to ours are observed for significantly lower Bond numbers. Further investigations may be needed in the future to understand this difference.

Accordingly, it is concluded that the flow properties of the alumina powder (GE15 and CR6) mixtures investigated using shear tests are controlled by the competition between the inter-particle interaction forces (Van der Waals and capillary contributions) and gravity via the Bond number.

4. Conclusion

The rheological properties of GE15 / CR6 alumina-based powder mixtures have been investigated using shear tests on a powder rheometer. The evolution of the flow index, ff_c, as a function of the powder mixture composition has been determined for pre-shear consolidation stress values fixed to 6 and 9 kPa. It appears that:

- All the points form a single curve whatever the pre-shear consolidation stress value adopted,
- The CR6 powder belongs to the "very cohesive" domain. For comparison, the GE15 powder belongs to the "easy flowing" one,
- It exists a threshold concentration of GE15 powder, C^*_{GE15}, around 30–45 wt%, below which the flow properties of the mixtures are always governed by the poor flow properties of the CR6 powder. For concentrations of GE15 above C^*_{GE15}, the flow index increases linearly with the increase in GE15 content introduced in the mixtures,
- It appears that adding a small amount of a "poor flowing" powder (CR6) into a mixture mostly based on a "good flowing" powder (GE15) is strongly detrimental to the flow properties of the mixture. Conversely, adding a large amount (up to around 40 wt%) of a "good flowing" powder (GE15) into a mixture mostly based on a "poor flowing" powder (CR6) keeps the flow properties of the mixture to a poor level.

Additional tests have shown that the trajectory representing the evolution of the flow index as a function of the composition of the mixtures does not depend on the mixing conditions or the preconditioning conditions (influence of the relative humidity level) of the powders before completing the shear tests.

Finally, it has been shown that the flow properties of the mixtures investigated are controlled by the competition between the interparticle interaction forces (Van der Waals and capillary contributions) and gravity via the Bond number.

References

[1] D. Schulze, Powders and Bulk Solids – Characterization, Storage and Flow, Springer, Berlin, 2008.
[2] L.Y. Leung, C. Mao, L.P. Chen, C.-Y. Yang, Precision of pharmaceutical powder flow measurement using ring shear tester – High variability is inherent to powders with low cohesion, Powder Technol. 301 (2016) 920–926.
[3] M. Leturia, M. Benali, S. Lagarde, I. Ronga, K. Saleh, Characterization of flow properties of cohesive powders – a comparative study of traditional and new testing methods, Powder Technol. 253 (2014) 406–423.
[4] R. Freeman, J.R. Cooke, L.C.R. Schneider, Measuring shear properties and normal stresses generated within a rotational shear cell for consolidated and non-consolidated powders, Powder Technol. 190 (2009) 65–69.
[5] R.M. Nedderman, Statics and Kinematics of Granular Materials, Cambridge University Press, New York, 1992.
[6] A.W. Jenike, Gravity flow of bulk solids, Bulletin 108, Engineering Experiment Station, University of Utah, 1961.
[7] J. Thomas, H. Schubert, Particle Characterization, Partec 79, Nuremberg, 1979.
[8] Y. Guérin, Nuclear Fuels,DEN Monographs, Editions du Moniteur, Paris, 2009.
[9] M. Capece, R. Ho, J. Strong, P. Gao, Prediction of powder flow performance using a multi-component granular Bond number, Powder Technol. 286 (2015) 561–571.
[10] M. Capece, K.R. Silva, D. Sunkara, J. Strong, P. Gao, On the relationship of inter-particle cohesiveness and bulk powder behavior – Flowability of pharmaceutical powders, Int. J. Pharm. 511 (2016) 178–189.
[11] http://www.baikowski.com/products.
[12] M.N. Rahaman, Ceramic Processing and Sintering, CRC Press, Taylor & Francis Group, Boca Raton, FL, 2003.
[13] G. Couarraz, J.L. Grossiord, G. Huang, Initiation à la rhéologie – Bases théoriques et applications expérimentales, Editions Lavoisier, Paris, 2014.
[14] H.G. Merkus, G.M.H. Meesters, Particulate Solids – Tailoring Properties for Optimal Performance, Particle Technology Series, vol. 19, Springer, London, 2014.
[15] Standard test method for shear testing of powders using the Freeman Technology FT4 powder rheometer shear cell, ASTM standard D7891-15.
[16] J.-P. Romagnan, Comprendre la mécanique, EDP Sciences, Les Ulis, 2011.
[17] C. Barataud, Utilisation de nouveaux liants organiques pour le pressage de pièces céramiques de robinetterie, PhD Thesis Université de Limoges, 2000.
[18] G. Bernard-Granger, Fabrication et caractérisation de céramiques à grains fins pour applications industrielles, Ability to conduct researches in physics, Université des Sciences et Technologies de Lille, 2006.
[19] L. Yang, J.H. Hu, K. Bai, Capillary and Van der Waals forces between microparticles with different sizes in humid air, J. Adhes. Sci. Technol. 30 (2016) 566–578.
[20] K.L. Mittal, R. Jaiswal, Particle Adhesion and Removal, John Wiley & Sons Inc, Hoboken, New Jersey, 2015.
[21] D. Megias-Alguacil, L.J. Gauckler, Capillary and Van der Waals forces between uncharged colloidal particles linked by a liquid bridge, Colloid Polym. Sci. 288 (2010) 133–139.
[22] D. Megias-Alguacil, L.J. Gauckler, Erratum to Capillary and Van der Waals forces between uncharged colloidal particles linked by a liquid bridge, Colloid Polym. Sci. 288 (2010) 1501–1502.
[23] J.N. Israelachvili, Intermolecular and Surface Forces, Elsevier, Burlington, Massachusetts, 2011.
[24] C. Hamaker, The London-Van der Waals attraction between spherical particles, Physica IV 10 (1937) 1058–1072.
[25] E.M. Lifshitz, The theory of molecular attractive forces between solids, Soviet Phys. JETP 2 (1956) 73–83.
[26] D. Tabor, R. Winterton, The direct measurement of normal and retarded Van der Waals Forces, Proc. R. Soc. London Ser. A 312 (1969) 435–450.
[27] R.D. Shannon, Refractive index and dispersion of fluorides and oxides, J. Phys. Chem. Ref. Data 31 (2002) 931–970.
[28] K.F. Young, Compilation of the static dielectric constant of inorganic solids, J. Phys. Chem. Ref. Data 2 (1973) 313–409.
[29] S. Vaudez, J. Léchelle, S. Berzati, J.-M. Heintz, Assessing the oxygen stoichiometry during the sintering of (U, Pu)O_2 fuel, J. Nucl. Mater. 460 (2015) 221–225.
[30] C. Mayer, C. Gatumel, H. Berthiaux, Mixing dynamics for easy flowing powders in a lab scale Turbula® mix, ChERD 95 (2015) 248–261.
[31] L. Legoix, C. Gatumel, M. Milhé, H. Berthiaux, Characterizing powders in order to determine their flow behavior in a mixer – from small scale observations to macroscopic in-mixer rheology for powders of various flowabilities, Powder Technol. 322 (2017) 314–331.

Nomenclature

σ_{SF}: Normal stress at pre-shear point
τ_{SF}: Shear stress at pre-shear point
σ: Normal stress at steady-state flow
τ: Shear stress at steady-state flow
μ: Static inter-particle friction coefficient
c: Cohesion
σ_1: Major principal stress
f_c: Unconfined yield stress
ϕ: Angle of internal friction
ϕ_{SF}: Angle of internal friction at steady state flow
σ_M: Normal stress representative of the center of the large Mohr semicircle
ff_c: Flow index
SSA^{BET}: Specific area of a powder measured using the BET method
d_{BET}: Equivalent crystallite diameter calculated from BET measurements
ρ_{th}: Theoretical density of alumina (3.98 g/cm^3)
FSD: Freely settled density of a given powder bed
TD: Tapped density of a given powder bed
I_{Carr}: Carr index of a given powder bed
R_H: Hausner ratio of a given powder bed
ε: Porous degree of a freely settled powder bed
ρ_{air}: Density of air at room temperature (1.2×10^{-3} g/cm^3)
E_c: Kinetic energy of an object in rotation
J: Moment of inertia of an object in rotation
ω: Speed of rotation applied to an object
E_m: Maximum kinetic energy applied to an object in rotation
ω_m: Maximum speed of rotation applied to an object
$|F_{ES}|$: Electrostatic force absolute value between two smooth spherical particles
D_1 *and* D_2: Diameters of both particles interaction
C_1 *and* C_2: Surface charges of both particles in interaction
ε: Relative dielectric constant of the medium where the interaction occurs
ε_0: Vacuum dielectric constant (8.90×10^{-12} C^2.N^{-1}.m^{-2})
λ: Distance between the centers of both particles
F_c: Capillary force between two smooth spherical particles connected by a water meniscus
R_1 *and* R_2: Radii of both particles in interaction
r_n *and* r_p: Radii of curvature of the water meniscus
β_1 *and* β_2: Filling angles of the water meniscus
θ_1 *and* θ_2: Contact angles of the water meniscus towards the surface of both particles
d: Separation distance between the surface of both particles
γ_{LV}: The surface tension of water (72.8 mN/m)
F_{VDW}: van der Waals force between two smooth spherical particles
$[A_{Al2O3-Al2O3}]^{air}$: Hamaker constant value for two smooth spherical alumina particles interacting in air
T: Absolute temperature
k: Boltzmann constant (1.38×10^{-23} J.K^{-1})
ε_1: Static relative dielectric constant of alumina (~10.1)
ε_3: Static relative dielectric constant of the interaction media (i.e. air, ~1)
h: Planck constant (6.62×10^{-34} J.s)
ν_e: Main frequency of electronic absorption positioned in the UV range (~3×10^{15} s^{-1})
n_1: Alumina refractive index in the visible range (~1.76 for a wavelength of 600 nm, taking into account only the real-part of the refractive index and neglecting absorption because alumina is transparent in the visible range, as demonstrated by sapphire)
n_3: Refractive index of the interacting medium in the visible range (i.e. air, ~1 for a wavelength of 600 nm)
B_{mix}: Bond number of a powder mixture
B_{ij}: Granular Bond number for particles i and j in interaction
ω_{ij}: Weighting functions for particles i and j in interaction
F_{ij}: Total interaction force for particles i and j in interaction
W_{ij}: Particle weight contribution for particles i and j in interaction
W_i *and* W_j: Weight for particles i and j in interaction
D_i *and* D_j: Diameter for particles i and j in interaction
ρ_i *and* ρ_j: Density for particles i and j in interaction
f_i^{SA} *and* f_j^{SA}: Fractional area for particles i and j in interaction